Lattice dynamical calculation of negative thermal expansion in ZrV_2O_7 and HfV_2O_7

R. Mittal[1,2] and S. L. Chaplot[2]
[1]*Juelich Centre for Neutron Science, IFF, Forschungszentrum Juelich, Outstation at FRM II, Lichtenbergstrasse 1, D-85747 Garching, Germany*
[2]*Solid State Physics Division, Bhabha Atomic Research Centre, Trombay, Mumbai 400085, India*
(Received 6 August 2008; revised manuscript received 6 October 2008; published 7 November 2008)

We report lattice dynamics calculations of negative thermal-expansion (NTE) behavior of ZrV_2O_7 family, extending our previous work on the ZrW_2O_8 family. The two families of compounds differ in terms of the oxygen coordination around the V/W atoms leading to differences in the nature of soft phonons under compression that are responsible for the NTE. Our calculations quantitatively reproduce the negative expansion over a range of temperatures. We also discuss the relation of the soft phonons with the phase transitions observed in the ZrV_2O_7 family. Especially, the calculations show a soft-phonon mode at a wave vector of $0.31\langle 1,1,0\rangle$, which is in excellent agreement with the known incommensurate modulation in ZrV_2O_7 below 375 K.

DOI: 10.1103/PhysRevB.78.174303 PACS number(s): 63.20.−e, 65.40.−b

I. INTRODUCTION

Large isotropic negative thermal expansion (NTE) from 0.3 to 1050 K was discovered[1] in cubic ZrW_2O_8. Since then many experimental and theoretical simulation studies[1–10] have been carried out to determine phonon spectrum and its relevance to NTE in framework solids. These compounds may be used to form composites that have specifically tailored thermal-expansion coefficients. Composites containing the NTE material ZrW_2O_8 have been examined[11,12] for low-thermal expansion and high conductivity for use in fiber-optic communication systems.

There has been considerable interest in the negative thermal-expansion properties of MV_2O_7 (M=Zr,Hf). Recent papers have described work on the structure and thermodynamic properties of these compounds using a combination of diffraction and spectroscopic techniques.[13–17] Powder and neutron diffraction, electron microscopy, and differential scanning calorimetry have been used to study structural changes in MV_2O_7 as a function of temperature. Like the ZrW_2O_8 family[1] (space group $P2_13$), the ZrV_2O_7 family[15,16] has a cubic crystal structure (though with a different space group $Pa\bar{3}$), and shows a large isotropic NTE. However, unlike the former, only the high-temperature phase of the latter shows NTE. The basic structure of MW_2O_8 and MV_2O_7 consists of corner-sharing MO_6 octahedra and WO_4/VO_4 tetrahedra. In case of MV_2O_7 each VO_4 tetrahedron shares three of its four O atoms with an MO_6 octahedron, while the fourth is shared with another VO_4 tetrahedron leading to a V_2O_7 group. All oxygen atoms in MV_2O_7 have twofold coordination, whereas in MW_2O_8 one of the oxygen atoms belonging to WO_4 tetrahedra is coordinated with only one W atom.

Earlier we reported[7–10] inelastic neutron scattering and lattice dynamical calculations to understand NTE in ZrW_2O_8, HfW_2O_8, $ZrMo_2O_8$, Cu_2O, and Ag_2O. We have now extended our studies to ZrV_2O_7 and HfV_2O_7, which have a different negative thermal-expansion behavior as compared to MW_2O_8. In this paper we report our calculation of NTE for the high-temperature phase (40 atoms per primitive cell). Below 375 K, ZrV_2O_7 first transforms to an incommensurate structure,[3] and then below 350 K, it further transforms to a $3\times3\times3$ superstructure[16] with cubic space group of $Pa\bar{3}$. Our calculations show a soft-phonon mode at a wave vector of $0.31\langle 1,1,0\rangle$, which could lead to the incommensurate phase transition. We also discuss the positive thermal expansion in the low-T phase though calculations are not attempted on its 1080 atoms primitive cell. Section II gives details about the lattice dynamical calculations, followed by the results and discussion and conclusions in Secs. III and IV, respectively.

II. LATTICE DYNAMICAL CALCULATIONS

The lattice dynamical calculation are performed using the following interatomic potentials:[18,19]

$$V(r)=\left\{\frac{e^2}{4\pi\varepsilon_0}\right\}\left\{\frac{Z(k)Z(k')}{r}\right\}+a\exp\left\{\frac{-br}{R(k)+R(k')}\right\}-\frac{C}{r^6}, \quad (1)$$

where r is the distance between the atoms k and k'. The first term is the long-range Coulombic attractive potential, the second is the Born-Mayer repulsion, and the third is the van der Walls attraction potential. The third term is applied only between oxygen atoms. Three body terms are not included in the potential although their contribution to some extent is mimicked by the two-body potential. For example, O-V-O and V-O-Zr bond angles are partly determined by the O-O and V-Zr potentials, respectively. The parameters of the interatomic potential are the effective charge $Z(k)$ and radius $R(k)$ of the atom type k. a=1822 eV and b=12.364. Partial charges of Z(Zr/Hf)=2.2, Z(V)=2.75, and Z(O)=−1.1 and radii parameters R(Zr/Hf)=1.17 Å, R(V)=0.90 Å, and R(O)=2.05 Å are used. The ionic radius of zirconium (=86 pm) and hafnium (=85 pm) coordinated by six nearest oxygen atoms are essentially the same. Therefore the same radius parameter is used for the Zr and Hf atoms. We have used the same potentials for both the Zr and Hf compounds in our previous studies on tungstates[9] also. The parameter C

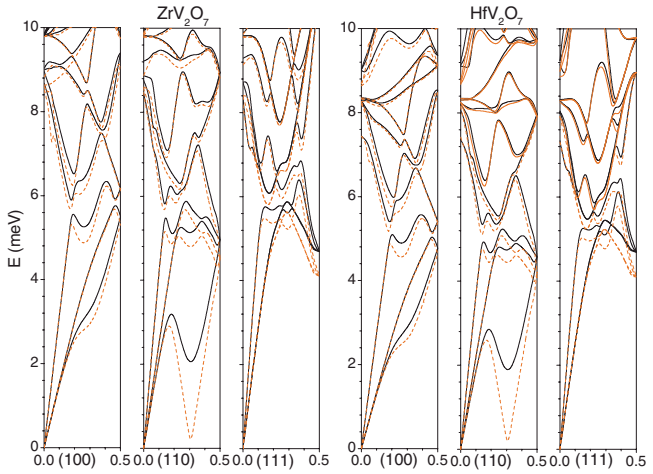

FIG. 1. (Color online) The calculated phonon-dispersion relation up to 10 meV for cubic ZrV_2O_7 and HfV_2O_7 along the (100), (110), and (111) directions. The solid and dashed lines correspond to ambient pressure and 3 kbar, respectively.

was set to 100 eV/Å^6. Because of the covalent nature of the V-O bond, a stretching term has been included further in the potential model.

$$V(r) = -D\exp[-n(r-r_0)^2/(2r)]. \quad (2)$$

Both the potentials of Eqs. (1) and (2) are combined in all the calculations. The parameters of covalent potential are $D=2.0$ eV, $n=22.0$ Å^{-1}, and $r_0=1.68$ Å. The polarizibility of the oxygen atoms is introduced in the framework of the shell model[20,21] with the shell charge $Y(\mathrm{O})=-1.6$ and shell-core force constant $K(\mathrm{O})=90$ eV/Å^2. The potential parameters satisfy the static and dynamic equilibrium conditions of the lattice. At any pressure the enthalpy is minimized at $T=0$ with respect to the lattice parameters and the atomic positions. The equilibrium structures thus obtained are used in lattice-dynamics calculations in the quasiharmonic approximation.

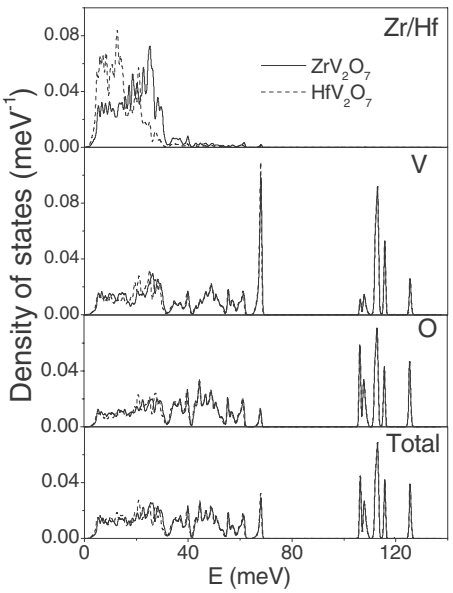

FIG. 2. Calculated partial density of states of various atoms in ZrV_2O_7 and HfV_2O_7.

TABLE I. Comparison of the calculated (at 0 K) and experimental structural parameters in the cubic phase of ZrV_2O_7 (at 387 K) (Ref. 16) and HfV_2O_7 (at 480 K) (Ref. 15). For the space group $Pa\bar{3}$, the Zr/Hf, V, O1, and O2 atoms are located at (0, 0, 0), (x,x,x), (x,y,z), and (0.5, 0.5, 0.5), respectively, and their symmetry equivalent positions. Since the ionic radii of Hf and Zr are nearly the same, we have used the same potentials for both the Zr and Hf compounds. Therefore the calculated structures for both ZrV_2O_7 and HfV_2O_7 are the same.

		Expt.		Calc.
		ZrV_2O_7	HfV_2O_7	
	a (Å)	8.8194	8.7862	8.914
Zr/Hf	x	0.0	0.0	0.0
V	x	0.3865	0.381	0.390
O1	x	0.4366	0.437	0.439
	y	0.2052	0.205	0.213
	z	0.4072	0.408	0.419
O2	x	0.5	0.5	0.5

In order to obtain the wave vectors in the Brillouin zone for the calculation of the density of states and thermal expansion (as discussed below), the cubic primitive reciprocal cell is partitioned with a $18\times18\times18$ mesh. We obtain[22] sets of mesh points that are equivalent by symmetry and retain only one point in each set with a weight equal to the number of points in the set. In this way, we used 165 independent wave vectors with suitable weighting factors. The calculations are carried out using the DISPR (Ref. 23) software package developed at Trombay.

Thermal expansion in insulators occurs mainly due to anharmonic nature of phonon excitations. NTE or thermal compression is favored if the compression leads to a decrease in some of the phonon frequencies which in turn leads to an increase in vibrational entropy. Quantitatively, in the quasiharmonic approximation the volume thermal-expansion coefficient is given by

$$\alpha_V = \frac{1}{BV}\sum_i \Gamma_i C_{Vi}(T), \quad (3)$$

where V is the unit-cell volume, B is the bulk modulus, $\Gamma_i(=d\ln E_i/d\ln V)$ and C_{Vi} are the mode-Grüneisen parameter and specific-heat contribution, respectively, of the phonons in state $i(=\mathbf{q}j)$ of frequency E_i. It is worth noting that anomalous thermal-expansion occurs because Γ_i, which reflects the dependence of the frequency E_i on volume, is very different for different modes. Otherwise, the coefficient of thermal expansion would closely follow the variation in the specific heat, as happens in many materials. The detailed procedure for the lattice dynamical calculations and various thermodynamic properties is given in our previous publications.[18,19]

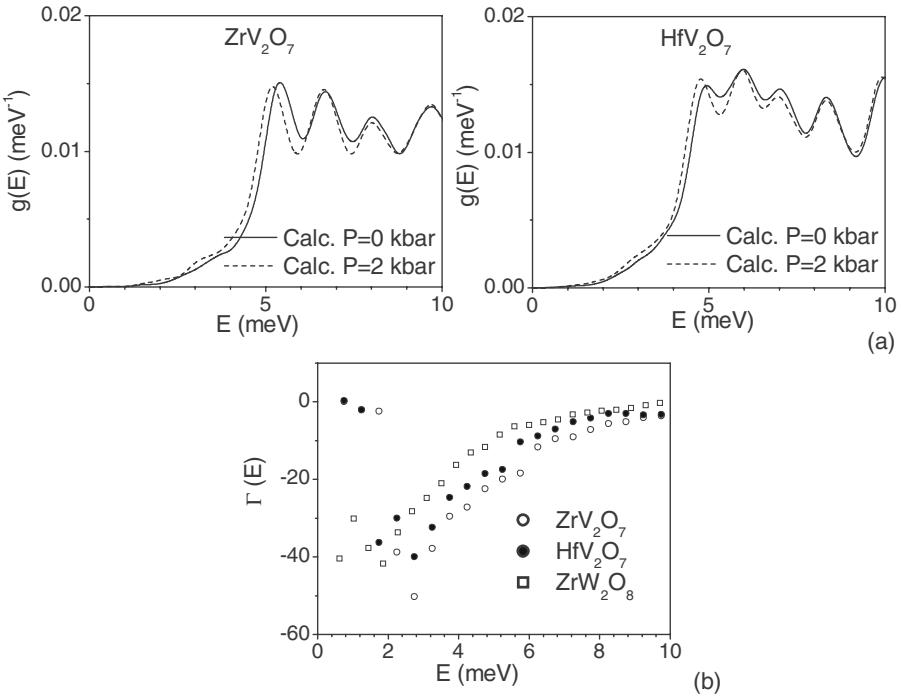

FIG. 3. (a) Calculated pressure variation of phonon density of states up to 10 meV in ZrV_2O_7 and HfV_2O_7. (b) Calculated Grüneisen parameter $\Gamma(E)$ averaged over phonons of energy E. For comparison, the calculated values (Ref. 9) of $\Gamma(E)$ for ZrW_2O_8 are also shown.

III. RESULTS AND DISCUSSION

The temperature dependent x-ray diffraction measurements[3,13,16] for ZrV_2O_7 and HfV_2O_7 show that the phase below 350 K corresponds to a primitive $3\times3\times3$ superstructure phase of $Pa\bar{3}$ space-group symmetry while the high-temperature phase above about 375 K corresponds to the normal parent structure. The intermediate incommensurate phase[3] is characterized by a modulation wave vector of $0.314\langle110\rangle$.

The high-T cubic phase of MV_2O_7 has 40 atoms in the primitive cell and thus 120 phonon modes at each wave vector. The calculated pressure dependence of the phonon-dispersion relation in the high-T phase of MV_2O_7 in the quasiharmonic approximation is shown in Fig. 1 up to 10 meV. The significant larger mass of Hf (178.49 amu) in HfV_2O_7 in comparison to Zr (91.22 amu) in ZrV_2O_7 results in slightly lower phonon energies in HfV_2O_7. Large softening with pressure is observed for the phonon branches lying in the energy range of 2.5–9 meV. The transverse-acoustic modes along the (100) direction do not show large softening, which is in contrast to ZrW_2O_8. The maximum softening occurs for transverse-acoustic mode at $0.31\langle110\rangle$. These modes have been calculated in the high-T phase in the quasiharmonic approximation. The soft modes at $0.31\langle110\rangle$ stabilize in the high-T phase due to anharmonicity and freeze in the intermediate incommensurate phase. Freezing of these soft modes at the $0.31\langle110\rangle$ points in the reciprocal space at low temperature leads to the known incommensurate phase.[3] We note that the calculated soft-mode wave vector is in excellent agreement with the observed[3] incommensurate modulation. Subsequent freezing of the soft modes at the $\langle1/3,1/3,0\rangle$ points in the reciprocal space at lower temperature could lead to the known $3\times3\times3$ superstructure transition.[16] Once the $\langle1/3,1/3,0\rangle$ points become lattice points due to the phonon freezing, other points such as $\langle1/3,0,0\rangle$ and $\langle1/3,1/3,1/3\rangle$ would also become lattice points due to the symmetry of the low-T phase even though the modes at the latter points are not soft in the high-T phase.

The experimental Raman data[14,17] have been obtained from polycrystalline samples in the low-temperature phase. The range of phonon frequency in the high-temperature phase is expected to be same as that in the low-temperature phase. The calculated range (Fig. 2) of phonon frequencies in the high-temperature phase of ZrV_2O_7 and HfV_2O_7 is nearly same as that obtained from the experimental data[14,17] in the low-temperature phase. The potential reproduces the equilibrium crystal structure (Table I) and other dynamical properties quite satisfactorily as discussed later.

The contribution of various atoms in the lattice to the phonon vibrations at various energies is illustrated by the partial density of states shown in Fig. 2, in both the Hf and

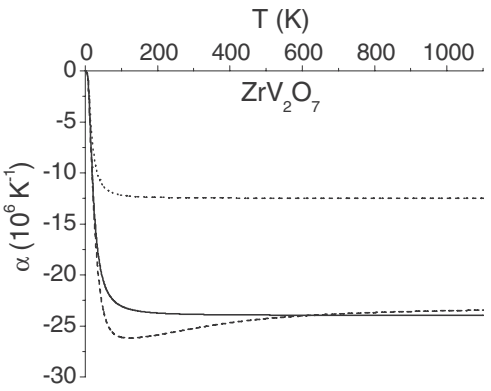

FIG. 4. The calculated volume thermal expansion (solid line) in the cubic ZrV_2O_7 along with separate contributions from the two lowest phonon branches (dotted line) and all the phonons below 9 meV (dashed line).

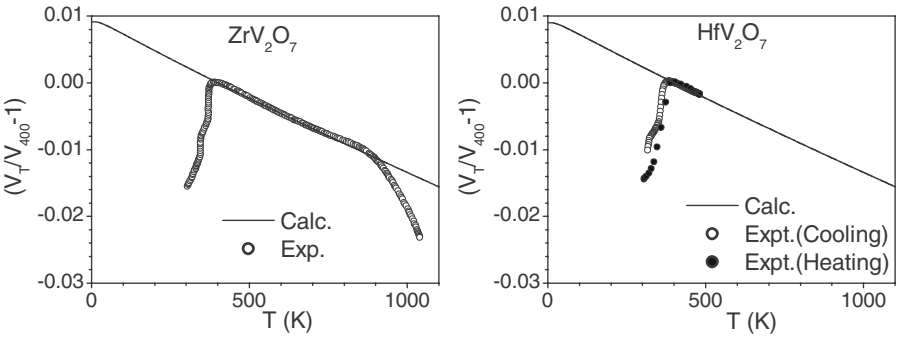

FIG. 5. Comparison between the calculated and experimental thermal expansion behaviors of ZrV_2O_7 (Ref. 3) and HfV_2O_7 (Ref. 15). The low-temperature phase of MV_2O_7 (M=Zr,Hf) below about 400 K has positive thermal-expansion coefficient. The calculations have been carried out in high-temperature phase.

Zr compounds. The Zr and Hf atoms contribute in energy range of 0–50 meV, while the vanadium and oxygen atoms contribute in the entire energy range up to 130 meV. Above 105 meV the contributions are mainly due to V-O stretching modes. The Zr-O and Hf-O stretching modes occur around 30–35 and 25–30 meV, respectively. The significant larger mass of Hf (178.49 amu) in HfV_2O_7 in comparison to Zr (91.22 amu) in ZrV_2O_7 give rise to the shift toward lower energies in the total density especially at low energies.

The calculated pressure dependence of phonon spectra is used for the calculation of the Grüneisen parameter $\Gamma(E)$, averaged for all phonons of energy E, in Fig. 3(b) for cubic ZrV_2O_7 and HfV_2O_7. Above 10 meV, the $\Gamma(E)$ values are small and lie between −1 and 1. The cubic HfV_2O_7 has slightly lower values of $\Gamma(E)$ in comparison to ZrV_2O_7. This is similar to the trend deduced from the analysis of the thermal expansion and specific heat data[4] in cubic ZrW_2O_8 and HfW_2O_8. Our calculated values of $\Gamma(E)$ for ZrW_2O_8 are also shown in Fig. 3(b) and show a similar variation as in ZrV_2O_7.

Our calculation of the temperature dependence of the volume thermal-expansion coefficient (Fig. 4) indicates that in cubic ZrV_2O_7 almost all the NTE (about 95%) is contributed from the phonon modes below 9 meV, among which nearly 50% of the NTE arises from just two lowest modes. The absolute value of thermal-expansion coefficient for HfV_2O_7 is slightly smaller in comparison with ZrV_2O_7. The comparison between the calculated and experimental data[3,15] for cubic ZrV_2O_7 and HfV_2O_7 is shown in Fig. 5. The agreement between our calculations and experimental data is excellent in the high-T phase between 400 and 900 K. In the low-T phase below 400 K, the soft phonons of the high-T phase would freeze and may no longer have the negative Grüneisen parameters. The low-T phase has positive thermal-expansion coefficient. Above 900 K, the experimental data show a sharp drop in the volume at about 900 K, which probably signifies another phase transition.

In Fig. 6 we show the contribution of various phonons to the thermal expansion as a function of phonon energy at 500 K for ZrV_2O_7 and HfV_2O_7. The maximum negative contribution to α_V at 500 K is from the modes of energy from 4 to 7 meV. The nature of the phonons may also be visualized from the calculated partial contributions of the phonons of different energies to the mean-square vibrational amplitude (Fig. 7) of the various atoms. The modes up to 2 meV involve equal displacement of all the atoms, which correspond to the acoustic modes. Above 2–15 meV, the O1 and O2 atoms connected to ZrO_6 and VO_4 have larger amplitudes in comparison of Zr and V. Further, the various oxygen atoms constituting the tetrahedra have nearly same values of their vibrational amplitudes, which indicate translation and rotation of the ZrO_6 octahedral and VO_4 tetrahedral units. This is quite different from cubic ZrW_2O_8 where the important modes around 4 meV involved the oxygen atoms constituting the WO_4 and ZrO_6, and these oxygen atoms have significantly different values of their vibrational amplitudes, indicating distortions of ZrO_6 octahedral and WO_4 tetrahedral units.

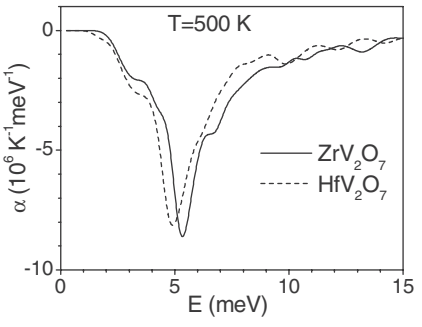

FIG. 6. Contribution of phonons of energy E to the volume thermal expansion as a function of E at 500 K.

IV. CONCLUSIONS

We have reported the lattice dynamical calculations of NTE in ZrV_2O_7 and HfV_2O_7. Our estimates of NTE coefficient agree very well with available experimental data. Our

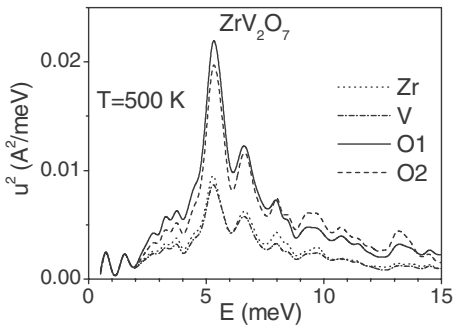

FIG. 7. The calculated contribution to the mean squared amplitude of various atoms arising from phonons of energy E at T =500 K in ZrV_2O_7. The atoms are labeled as indicated in Table I.

calculations show that phonon modes of energy from 4 to 7 meV are major contributors to NTE. These important phonon modes involve translations and librations of ZrO_6 octahedral and VO_4 tetrahedral units, which significantly soften on compression of the lattice and lead to the thermal compression. The maximum softening in the high-T phase occurs at $0.31\langle 1,1,0\rangle$, which is near $\langle 1/3,1/3,0\rangle$, and the freezing of these modes at low temperature could lead to the known incommensurate phase below 375 K, and then below 350 K to the $3\times3\times3$ superstructure. The phonon modes involved in NTE in ZrV_2O_7 are found to be quite different from those involved in cubic ZrW_2O_8.

[1] T. A. Mary, J. S. O. Evans, T. Vogt, and A. W. Sleight, Science **272**, 90 (1996).
[2] A. L. Goodwin and C. J. Kepert, Phys. Rev. B **71**, 140301(R) (2005).
[3] R. L. Withers, J. S. O. Evans, J. Hanson, and A. W. Sleight, J. Solid State Chem. **137**, 161 (1998).
[4] Y. Yamamura, N. Nakajima, and T. Tsuji, Phys. Rev. B **64**, 184109 (2001).
[5] J. W. Zwanziger, Phys. Rev. B **76**, 052102 (2007).
[6] C. Lind, A. P. Wilkinson, Z. Hu, S. Short, and J. D. Jorgensen, Chem. Mater. **10**, 2335 (1998).
[7] R. Mittal, S. L. Chaplot, H. Schober, and T. A. Mary, Phys. Rev. Lett. **86**, 4692 (2001).
[8] R. Mittal and S. L. Chaplot, Phys. Rev. B **60**, 7234 (1999).
[9] R. Mittal, S. L. Chaplot, A. I. Kolesnikov, C. K. Loong, and T. A. Mary, Phys. Rev. B **68**, 054302 (2003).
[10] R. Mittal, S. L. Chaplot, S. K. Mishra, and Preyoshi P. Bose, Phys. Rev. B **75**, 174303 (2007).
[11] D. A. Fleming, D. W. Johnson, and P. J. Lemaire, U.S. Patent No. 5,694,503 (2 December 1997); H. Holzer and D. C. Dunand, J. Mater. Res. **14**, 780 (1999).
[12] C. Verdon and D. C. Dunand, Scr. Mater. **36**, 1075 (1997).
[13] T. Hisashige, T. Yamaguchi, T. Tsuji, and Y. Yamamura, J. Ceram. Soc. Jpn. **114**, 607 (2006).
[14] U. L. C. Hemamala, F. El-Ghussein, A. M. Goedken, B. Chen, Ch. Leroux, and M. B. Kruger, Phys. Rev. B **70**, 214114 (2004).
[15] C. Turquat, C. Muller, E. Nigrelli, C. Leroux, J.-L. Soubeyroux, and G. Nihoul, Eur. Phys. J.: Appl. Phys. **10**, 15 (2000).
[16] J. S. O. Evans, J. C. Hanson, and A. W. Sleight, Acta Crystallogr., Sect. B: Struct. Sci. **54**, 705 (1998).
[17] T. Sakuntala, A. K. Arora, V. Sivasubramanian, Rekha Rao, S. Kalavathi, and S. K. Deb, Phys. Rev. B **75**, 174119 (2007).
[18] S. L. Chaplot, N. Choudhury, S. Ghose, M. N. Rao, R. Mittal, and P. Goel, Eur. J. Mineral. **14**, 291 (2002).
[19] R. Mittal, S. L. Chaplot, and N. Choudhury, Prog. Mater. Sci. **51**, 211 (2006).
[20] G. Venkataraman, L. Feldkamp, and V. C. Sahni, *Dynamics of Perfect Crystals* (MIT, Cambridge, MA, 1975).
[21] P. Bruesch, *Phonons: Theory and Experiments I* (Springer-Verlag, Berlin, 1982).
[22] S. L. Chaplot, Phys. Rev. B **36**, 8471 (1987).
[23] S. L. Chaplot (unpublished).